Ab Initio Polariton Transport Dynamics with the Classical Path Approximation

Benjamin X. K. Chng,[†] Braden M. Weight,[‡] M. Elious Mondal,[¶] and Pengfei Huo[*,¶,§,‖]

[†]*Department of Physics and Astronomy, University of Rochester, Rochester, NY 14627, U.S.A.*
[‡]*Theoretical Division, Center for Integrated Nanotechnologies, Los Alamos National Laboratory, Los Alamos, NM, 87545, U.S.A.*
[¶]*Department of Chemistry, University of Rochester, Rochester, NY 14627, U.S.A.*
[§]*The Institute of Optics, Hajim School of Engineering, University of Rochester, Rochester, NY 14627, U.S.A.*
[‖]*Center for Coherence and Quantum Optics, University of Rochester, Rochester, New York 14627, U.S.A.*

E-mail: pengfei.huo@rochester.edu

Abstract

We present an *ab initio* framework for simulating polariton transport dynamics based on the classical path approximation (CPA). The quantum dynamics of polariton transport involves simulating many electronic degrees of freedom—often numbering in the hundreds to thousands—making a fully ab initio treatment of the dynamics computationally expensive. We demonstrate that the CPA, which reduces the number of electronic structure computations needed, is well-suited for polaritonic systems because the collective light–matter coupling leads to vanishing excited-state forces. Benchmark comparisons between CPA and full evaluation of the excited state forces show excellent agreement for polariton transport results in model light-matter systems, such as wave packet velocities and mean-squared displacements. Further, ab initio simulations of polariton transport using the CPA reproduce key physical trends that are observed in experiments with BODIPY molecules. Our work thus establishes the CPA as a highly efficient tool for ab initio investigations of transport and energy flow in hybrid light–matter systems.

KEYWORDS: *Polariton Transport, ab initio on-the-fly simulations, Exciton Polariton, Light-Matter Interactions, Quantum Electrodynamics*

Polaritons, quasi-particles formed by the hybridization of excitons and photons, have recently been shown to enhance energy transport significantly. Recent experiments have reported large group velocities for polaritons.[1–6] Further, Ref. 2 shows that the velocities of the polariton wave packet depend on the cavity quality factor $\mathcal{Q}$. Although $\mathcal{Q}$ does not directly impact polariton's dispersion relation, it affects the polariton's lifetime (thus also influences polariton coherence[7,8]) and can significantly impact transport dynamics.[9] The exciting experimental progress in this area also sparked intensive theoretical investigations[3,7,10–25] on polariton transport, using both quantum dynamics simulations[3,9,21] and analytic theories.[17,19] Nonetheless, most of these investigations are limited to simple system-bath type of exciton model systems, with a few exceptions.[11,18]

On-the-fly quantum dynamics simulation is one of the most desirable approaches to explicitly describe the *ab-initio* polariton non-adiabatic dynamics in realistic molecule-cavity hybrid systems. Specifically, one requires both ground *and excited* state energies and all state-to-state electric transition and permanent dipole moments, in addition to various response properties of the electronic system such as nuclear gradients of the energies, transition dipole moments, and non-adiabatic couplings,[26] all at each time-step. These evaluations of these gradients make the quantum dynamics simulations in the collective coupling regime computationally prohibitive. In excited state simulations,

a widely used approximation[27–30] solves the non-adiabatic Time-Dependent Schrodinger Equation (TDSE) on the ground state classical trajectory. On the other hand, the quantum subsystem would still evolve based on the TDSE for the quantum subsystem. The above-mentioned approximation is often referred to as the classical path approximation (CPA).

In this letter, we investigate the validity of the CPA by simulating the quantum dynamics of the generalized Holstein-Tavis-Cummings (HTC) Hamiltonian. The dynamics with CPA show excellent agreement compared to results obtained from the full evaluation of the non-adiabatic and cavity-mediated forces. Further ab initio simulations of polariton transport for BODIPY molecules coupled to a FP cavity[2] are performed in this framework under CPA, and results reproduce key experimental features, such as the polariton wavepacket's mean-squared displacement (MSD), from previous experimental work.[2] The classical-path approximation (CPA),[27–29] drastically reduces the cost of the electronic structure calculations and enables large-scale, accurate quantum dynamics simulations.

The molecular Hamiltonian is expressed as

$$\begin{aligned}\hat{H}_n =& \hat{T}_{\mathbf{R}_n} + E_g(\mathbf{R})|g_n(\mathbf{R}_n)\rangle\langle g_n(\mathbf{R}_n)| \\ &+ E_e(\mathbf{R}_n)|e_n(\mathbf{R}_n)\rangle\langle e_n(\mathbf{R}_n)|,\end{aligned} \tag{1}$$

where $\hat{T}_{\mathbf{R}_n}$ is the nuclear kinetic energy for molecule n, and $|g_n(\mathbf{R}_n)\rangle$ and $|e_n(\mathbf{R}_n)\rangle$ as the ground state and excited states, respectively. We use the generalized Tavis-Cummings (GTC) Hamiltonian[3,31–33] to describe the collective light-matter coupling between molecules and the cavity modes, as follows

$$\begin{aligned}\hat{H} =& \sum_{n=1}^{N}\hat{H}_n + \sum_{\mathrm{k}_\parallel}\hbar\omega_{\boldsymbol{k}}(\hat{a}^\dagger_{\boldsymbol{k}}\hat{a}_{\boldsymbol{k}} + \frac{1}{2}) \\ &+ \sum_{\boldsymbol{k},n}\sqrt{\frac{\omega_{\boldsymbol{k}}}{2}}\boldsymbol{\lambda}\cdot\hat{\boldsymbol{\mu}}_n(\mathbf{R}_n)(\hat{a}_{\boldsymbol{k}}e^{i\boldsymbol{k}_\parallel\cdot\mathbf{x}_n} + \hat{a}^\dagger_{\boldsymbol{k}}e^{-i\boldsymbol{k}_\parallel\cdot\mathbf{x}_n}),\end{aligned} \tag{2}$$

where $\boldsymbol{\lambda}_{\boldsymbol{k}} = \sqrt{\frac{1}{\epsilon_0 V}}\hat{\mathbf{e}}_{\boldsymbol{k}}$ is the coupling for a given mode and wavevector $\boldsymbol{k}$, $\lambda = |\boldsymbol{\lambda}_{\boldsymbol{k}}|$, and $\hat{\boldsymbol{\mu}}_n(\mathbf{R}_n)$ is the dipole operator of the n_{th} molecule, where x_n is the center of mass location of the n_{th} molecule.[31]

We model the FP cavity with an open direction x characterized by an in-plane wavevector $k_\parallel$, and one confined direction z where $k_\perp$ is the wavevector of the fundamental mode confined between two cavity mirrors, perpendicular to the mirror surface. The frequency of the cavity mode is given by

$$\hbar\omega_{\boldsymbol{k}} = \hbar c\sqrt{k_\parallel^2 + k_\perp^2}, \tag{3}$$

where c is the speed of light. Furhter, $\hat{a}^\dagger_{\boldsymbol{k}}$ and $\hat{a}_{\boldsymbol{k}}$ are the photonic creation and annilaition operators for mode $\boldsymbol{k}$, respectively. We consider $k_\parallel$ with discrete (but still quasi-continuous) values $k_\alpha = \frac{2\pi}{NL}\alpha$, where the mode indexes $\alpha \in [-\frac{\mathcal{M}-1}{2}, ...0, ...\frac{\mathcal{M}-1}{2}]$, and $\mathcal{M}$ is the total number of cavity modes needed to capture the relevant energies for the hybrid system.

The transport dynamics occur in the single excitation subspace

$$|E_n(\mathbf{R})\rangle = |e_n(\mathbf{R}_n)\rangle\bigotimes_{m\neq n}|g_m(\mathbf{R}_m)\rangle\bigotimes_{k_\alpha}|0_{k_\alpha}\rangle \tag{4a}$$

$$|k_\alpha\rangle = \bigotimes_n|g_n(\mathbf{R})\rangle\bigotimes_{k_\parallel\neq k_\alpha}|0_{k_\parallel}\rangle\otimes|1_{k_\alpha}\rangle\,, \tag{4b}$$

where $|E_n\rangle$ is the singly excited state for the n_{th} molecule located at x_n, $|k_\alpha\rangle$ is the 1-photon-dressed ground state with photonic momentum $\hbar k_\alpha$.

We use $\mathcal{L}$-MFE dynamics approach[34–36] to simulate the polariton transport quantum dynamics in a lossy cavity. This approach describes the exciton-photonic degrees of freedom (DOF) quantum mechanically

$$|\psi(t)\rangle = \sum_{n=1}^{N}c_n(t)\,|E_n(\mathbf{R}(t))\rangle + \sum_\alpha c_\alpha(t)\,|k_\alpha\rangle\,. \tag{5}$$

The polariton quantum dynamics is propagated with

$$i\hbar\frac{\partial}{\partial t}|\psi(t)\rangle = \hat{H}_{\mathrm{Q}}(\mathbf{R})|\psi(t)\rangle, \tag{6}$$

where $|\psi(t)\rangle$ is represented using Eq. 5, $\hat{H}_{\mathrm{Q}} = \hat{H} - \sum_n\hat{T}_{\mathbf{R}_n}$ is the quantum subsystem Hamiltonian that including excitonic and photonic DOFs (without the nuclear kinetic energy), and the EOM is numericallly solved using RK4 algorithm. Cavity loss is simulated through Lindblad dynamics using a stochastic approach,[34] assuming identical loss rates Γ_{c} for all cavity modes k_α. We define the cavity quality factor at normal incidence ($k_\parallel = 0$) as $\mathcal{Q} = \hbar c k_\perp/\Gamma_{\mathrm{c}}$.

Under the mixed quantum-classical dynamics ap-

proximation, the nuclear force is

$$\mathbf{F}_n = -\nabla_n E_g(\mathbf{R}_n) - |c_n(t)|^2 \nabla_n [E_e(\mathbf{R}_n) - E_g(\mathbf{R}_n)], \\ - \sum_\alpha 2\mathrm{Re}[c_n^*(t) c_\alpha(t) e^{-ik_\alpha x_n}] \cdot \nabla_n \langle g_n | \boldsymbol{\lambda}_{\boldsymbol{k}} \cdot \hat{\boldsymbol{\mu}}_n | e_n \rangle \tag{7}$$

where $\nabla_n \equiv \partial/\partial \mathbf{R}_n$, and the excitation population on the molecule n is $|c_n(t)|^2$ (see Eq. 5). The second line of Eq. 7 accounts for the derivative due to the nuclear position dependence of the transition dipoles $\boldsymbol{\lambda}_{\boldsymbol{k}} \cdot \hat{\boldsymbol{\mu}}_n(\mathbf{R}_n)$, and we have only considered the transition dipole contributions. Further, we assume the center of the mass position of molecules is fixed during polariton transport dynamics. This is in agreement with the experimental setup because the molecules are hosted in the PMMA polymers[1,2] and kept immobilized. The same type of forces (Eq. 7) is also used in mapping-based semiclassical dynamics methods[35–42] and in the Gaussian wavepacket-based method,[43–45] and our following discussions on CPA could also be applied to those methods.

Despite the available nuclear gradients and speed up with the machine learning models,[46] in general, it is still expensive to compute these excited states' gradients, $\nabla_{\mathbf{R}_n} E_e(\mathbf{R}_n)$. Further, for gradient term with the transition dipole $\nabla_n \langle g_n | \boldsymbol{\lambda}_{\boldsymbol{k}} \cdot \hat{\boldsymbol{\mu}}_n(\mathbf{R}_n) | e_n \rangle$, it is also less straightforward to evaluate, although one can take advantage of the machine learning model.[46] It is thus ideal to find approximations to avoid explicitly computing these excited states and dipole-related derivatives.

We hypothesize that under the collective light-matter coupling and in polariton transport dynamics, CPA is an accurate approximation, such that one does not need to compute the excited states' gradients as long as polaritons are delocalized among many molecules. This is because throughout the dynamics polariton wavepacket is very delocalized, such that most of the $|c_n|^2$ are small, with $|c_n|^2 \sim 1/\mathcal{N}$, where $\mathcal{N}$ is the number of molecules transiently excited among a total of N molecules in the single excitation subspace. Under a truly collective regime for polariton transport dynamics, $|c_n|^2 \ll 1$ (for a large $\mathcal{N}$), and the excited states force contribution in Eq. 7 can be ignored. Similarly, the term related to the dipole derivative can be ignored if $|c_n| \ll 1$, given that $|c_\alpha| \leq 1$. This means that we can replace the force in Eq. 7 with

$$\mathbf{F}_n \approx -\nabla_n E_g(\mathbf{R}_n(t)), \tag{8}$$

meaning classical path approximation (Eq. 8) is naturally valid for polariton transport problems. The CPA version of the polariton transport EOM thus uses Eq. 6 for the quantum subsystem (excitonic and photonic) and uses Eq. 8 for the nuclei update.

For simplicity, we have ignored the derivative coupling term $\hat{\mathbf{d}}_n = \langle g_n | \nabla_{\mathbf{R}_n} | e_n \rangle$ and the Born-Oppenheimer corrections $\hat{D}_n = \langle g_n | \nabla^2_{\mathbf{R}_n} | e_n \rangle$ in Eq. 1, which will cause non-radiative relaxation from $|e_n\rangle$ to $|g_n\rangle$. These processes are less important for the ultra-fast polariton transport, as the transport dynamics measured from experiments are usually shorter than the molecular exciton lifetime for the molecules.[1,2] Further, CPA argument is also applicable for the derivative couplings because the forces for those terms scale as $-c_i^*(t) c_j(t) [\mathbf{d}_{ij} \cdot (E_j - E_i)]$ for electronic states i and j. Note that $\mathbf{d}_{ij}$ could be large (or even singular) but $\nabla V_{ij} = [\mathbf{d}_{ij} \cdot (E_j - E_i)]$ is always finite.

We first test the validity of CPA using a system-bath model for the excitonic Hamiltonian (Eq. 1), allowing us to perform the simulation with the full nuclear gradients so we can assess the validity of CPA. The Hamiltonian is

$$\hat{H}_n = (\hbar\omega_{\mathrm{ex}} + \lambda + \sum_\nu C_{n,\nu} \hat{R}_{n,\nu}) \otimes \hat{\sigma}_n^\dagger \hat{\sigma}_n \\ + \sum_\nu \Big(\frac{1}{2} \hat{P}_{n,\nu}^2 + \frac{1}{2} \omega_\nu^2 \hat{R}_{n,\nu}^2 \Big), \tag{9}$$

where $\hat{\sigma}_n^\dagger = |e_n\rangle\langle g_n|$ and $\hat{\sigma}_n = |g_n\rangle\langle e_n|$, $\hbar\omega_{\mathrm{ex}}$ is the exciton energy and $\lambda = \sum_\nu C_{n,\nu}^2/\omega_\nu$ is the reorganization energy. Details of the models are provided in the SI. The light-matter coupling term in Eq. 2 is replaced as $\sqrt{\omega_{\mathbf{k}}/2} \boldsymbol{\lambda}_{\boldsymbol{k}} \cdot \hat{\boldsymbol{\mu}}_n(\mathbf{R}_n) \to \hbar g_{\mathrm{c}} \sqrt{\frac{\omega_{\mathbf{k}}}{\omega_{\mathrm{c}}}} \cos\theta$ (where $\tan\theta = k_\parallel/k_\perp$). Here, we use $N = 10001$ molecules, $\mathcal{M}$ =141 cavity modes, a reorganization energy λ =37.2 meV, and a bath characteristic frequency ω_f =6.2 meV for the phonon bath with Drude-Lorentz spectral density. The simulation results were converged with 250 trajectories in the Ehrenfest dynamics, with details provided in the Supporting Information.

Fig. 1a presents the impact of varying cavity quality factor $\mathcal{Q}$ on v_g with a broadband excitation on the UP band (indicated with the gray Gaussian wavepacket in the inset of Fig. 1a), to model experimental conditions in Ref. 2. The results suggest that group velocity v_g increases with increasing $\mathcal{Q}$, with open circles correspond results using the full nuclear force expressions, and the open

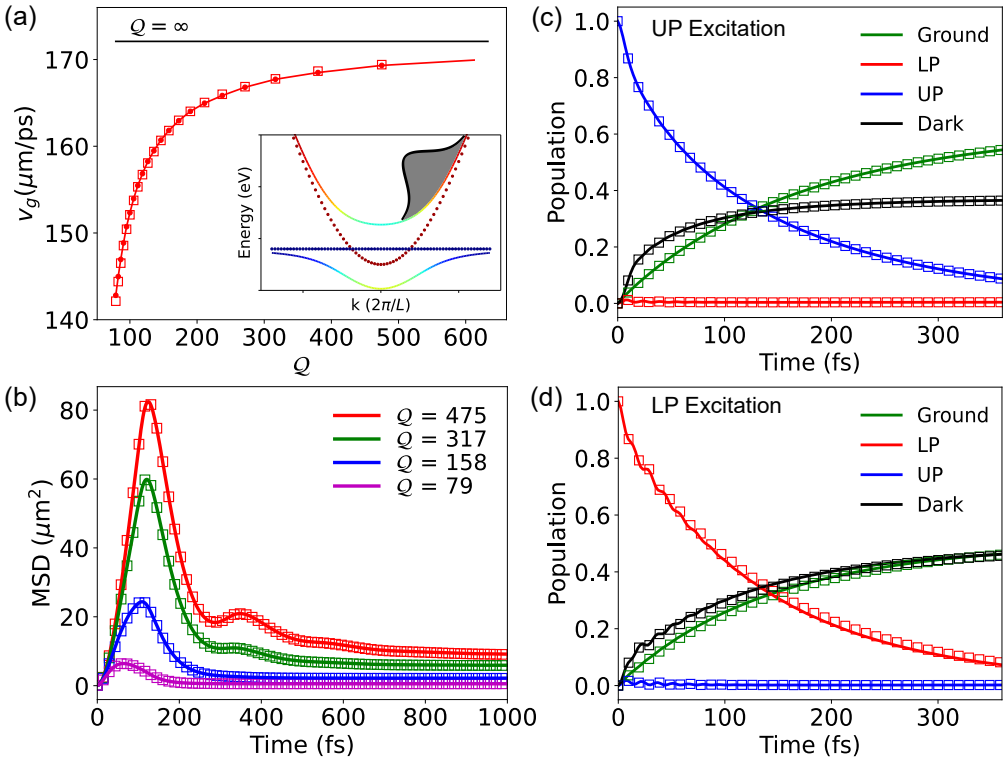

Figure 1: (a) Polariton group velocities v_g vs cavity quality factor $\mathcal{Q}$ for wavepackets computed with (filled circle) quantum forces on nuclei and (square) CPA. The inset figure shows the energy bandwidth used for the initial excitation in the UP branch that optimizes the localization of the polariton wavepacket. (b) Time-dependent transient MSD with UP initial excitation for different $\mathcal{Q}$. The populations of UP (blue), LP (red), dark (black), and ground states (green) in a cavity with $\mathcal{Q} = 475$ are presented, with (c) broadband UP excitation and (d) broadband LP excitation.

squares correspond to CPA results, which are in excellent agreement with the full simulation.

Fig. 1b shows the transient MSD of a polariton wavepacket

$$\sigma^2(t) = \langle\psi(t)|(\hat{x} - \langle\hat{x}\rangle)^2|\psi(t)\rangle, \qquad (10)$$

where $\langle\hat{x}\rangle$ is the centroid of the initial polariton wavepacket (at $t = 0$) in position space. For cavities with larger $\mathcal{Q}$, both the wavepacket's maximum MSD and the corresponding rise time increase. The initial rise of MSD is due to the photonic character of the polariton wavepacket, which is responsible for ballistic transport.[7] The dip in MSD right after the initial rise is linked to both the decay of the UP population to the dark states and to cavity loss, which are competing on a similar time scale.[9] The open circles denote MSDs simulated from full calculations, and the open squares are for MSDs computed with CPA. As we expect, the MSDs evaluated with the two wavepackets agree well with one another.

Fig. 1c and Fig. 1d present the population dynamics of the UP (blue), LP (red), and dark states (black) under broadband UP excitation and broadband LP excitation, respectively, with cavity quality factors of $\mathcal{Q} = 475$. The ground-state population (green) is also depicted. For N molecules and $\mathcal{M}$ cavity modes, there is a total of $\mathcal{M}$ different UP and LP states each (with different k_α), and $N - \mathcal{M}$ dark exciton states. The definitions of UP, LP, and Dark states are provided in Eqs. S14-15 of the Supporting Information. In Fig. 1c and Fig. 1d, the solid lines are populations for wavepackets evaluated with the full nuclear forces, while the open squares are populations evaluated with the CPA. We see that the populations with CPA are in excellent agreement with the full calculations.

Fig. 2a and Fig. 2b present the UP polariton wavepacket density and the dark exciton density in position space for broadband UP excitations. Over time, the UP (blue) wavepacket propagates outward from the center, primarily due to its *photonic character*, which exhibits ballistic transport (with v_g largely adopted from the derivative of the band). Due to exciton-phonon coupling, the

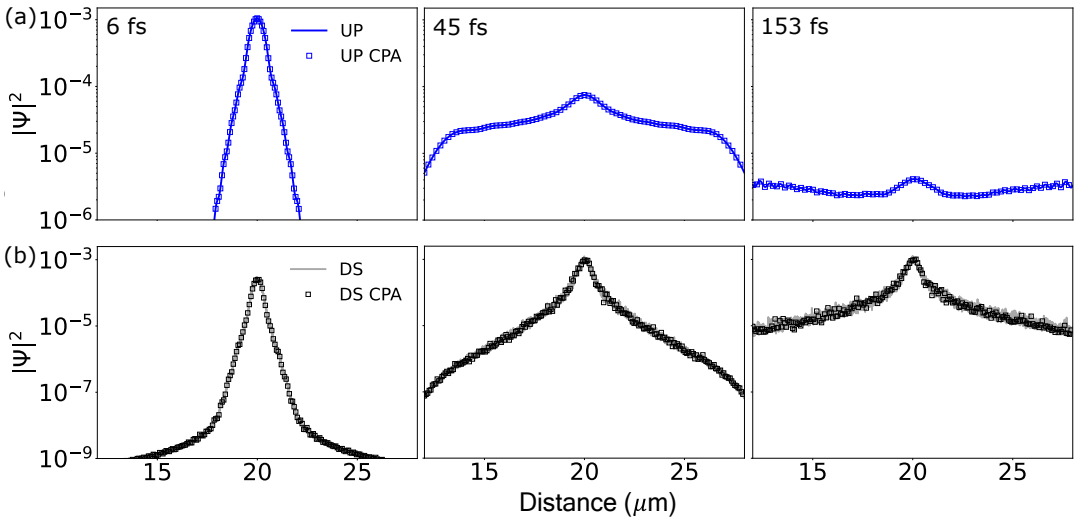

Figure 2: The wavepackets for broadband UP excitation in position space for (a) UP wavepacket and (b) dark-state wavepacket. The simulations were performed in an FP cavity with $\mathcal{Q} = 475$. The open squares denote the coefficients $|c_n(t)|^2$ evaluated using the CPA.

UP wavepackets transfer population to the dark state, resulting in an increase in the dark state (black) probability densities. The corresponding dark-state wavepacket itself is immobile (due to the zero group velocity of the exciton band), and its spatial expansion is purely due to the expanding UP wavepacket, which deposits populations to the dark exciton states in our simulations. With the full nuclear gradient expression, we can see that the polariton wavepacket remains delocalized among a large $\mathcal{N}$ sites, leading to a small magnitude of the expansion coefficients of excitons, $|c_n| \ll 1$, and making the CPA a valid approximation.

We also plot the UP wavepacket and the dark state wavepacket computed with the CPA, and they are denoted in Fig. 2a and Fig. 2b with open squares. The results from CPA match closely to the full simulations. It is clear from Fig. 2 that for each molecule at position x_n, the coefficients $|c_n(t)|^2 \ll 1$, satisfying the assumptions needed to use the CPA.

We further use the CPA approximation to simulate ab initio polariton transport dynamics for BODIPY coupled to the cavity. All electronic structure calculations conducted in this work were performed using Gaussian16.[47] The molecular ground state energies and forces were computed using the semi-empirical AM1 Hamiltonian[48] while the electronic excited states were computed using linear-response formalism in the Tamm-Dancoff approximation (TDA-AM1), with our in-house Python code[49] interfacing with the Gaussian package. Details are provided in the supporting Information.

Fig. 3 presents ab initio simulations of the polariton transmission spectroscopy and transport dynamics of BODIPY molecules. The experimental investigation of the same system has been done in Ref. 2). The molecular ground state energies and forces were computed using the semi-empirical AM1 Hamiltonian[48] while the excited states' energy and dipoles of these organic molecules were computed using linear-response formalism in the Tamm-Dancoff approximation (TDA-AM1), with our in-house Python code interfacing with the Gaussian package.

Fig. 3a and Fig. 3b show the ab initio simulation of transmission polariton spectra, with $N = 108$ BODIPY molecules coupled to $\mathcal{M} = 51$ FP cavity modes for $\sqrt{N}\lambda = 0.01$ a.u. and $\sqrt{N}\lambda = 0.02$ a.u., respectively. Indeed, the Rabi splitting is enlarged if one increases collective light-matter couplings. The k-resolved (angle-resolved) transmission spectra are computed with

$$\mathcal{T}_{\pm}(\omega, k_\alpha) = \left\langle \mathcal{N}_{\pm,k_\alpha} \cdot \delta(\hbar\omega - \mathcal{E}_{\pm,k_\alpha}(\mathbf{R})) \right\rangle_{\mathbf{R}} \quad (11)$$

where $\mathcal{E}_{\pm,k_\alpha}(\mathbf{R})$ is the polariton energy at a given k_α for the UP (+) and LP (−) band, $|\Phi_{\pm,k_\alpha}(\mathbf{R})\rangle$ is the polariton eigenstate, and $\mathcal{N}_{\pm,k_\alpha} = \langle \Phi_{\pm,k_\alpha}(\mathbf{R})|\hat{a}^\dagger_{\mathbf{k}}\hat{a}_{\mathbf{k}}|\Phi_{\pm,k_\alpha}(\mathbf{R})\rangle$ is the photon number expectation value under the polariton state. The polaritonic density of states (delta function) was weighted by the photonic character for that polariton polariton branch to give the transmission spectra. The delta function was broadened

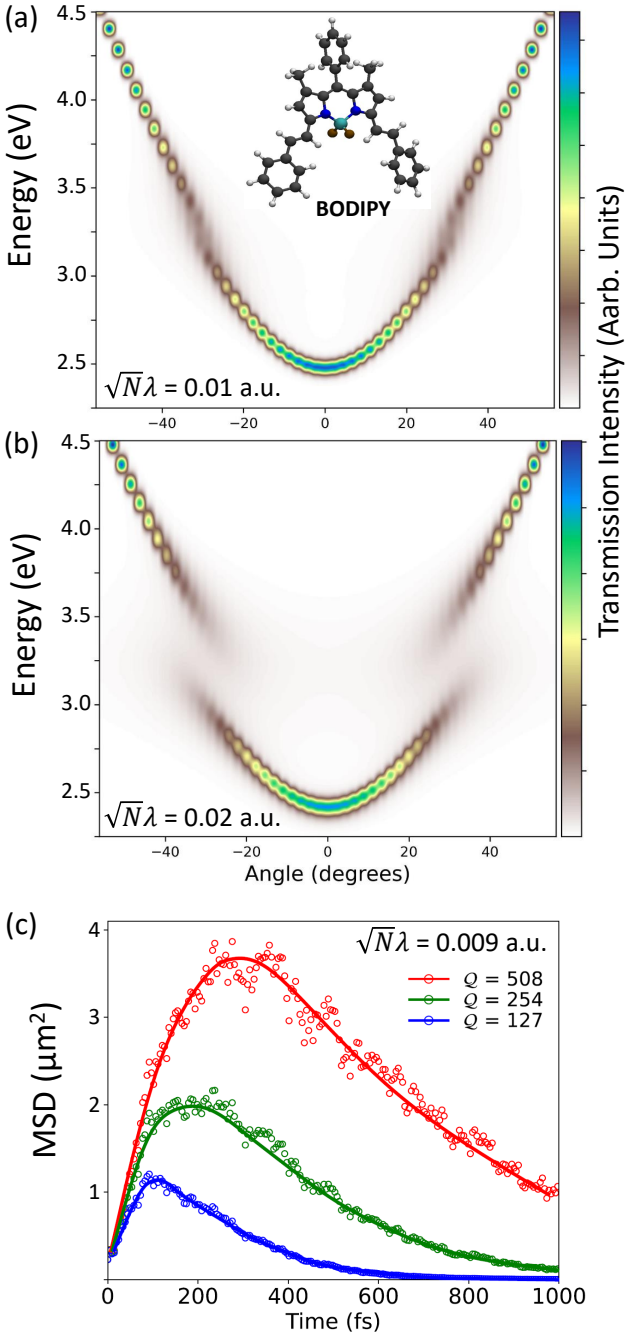

Figure 3: (a,b) Transmission spectroscopy of $N = 108$ BODIPY molecules coupled to $\mathcal{M} = 51$ cavity modes at collective light-matter coupling strength $\sqrt{N}\lambda =$ (a) 0.01 and (b) 0.02 a.u. The cavity frequency at 0 ω_c = 2.50 eV. (c) Mean-squared displacement (MSD) of the polariton wave packet over time for various cavity quality factors $Q =$ (blue, bottom) 127, (green, middle) 254, and (red, top) 508 for initial excitation to the upper polariton with collective light-matter coupling strength $\sqrt{N}\lambda \approx 0.009$ a.u., corresponding to $\Omega_R \approx 260$ meV at the resonant condition between light and matter.

with a Gaussian function of width $\sigma \approx k_B T = 26$ meV (room temperature). The ensemble average $\langle ... \rangle_{\mathbf{R}}$ represents an average over geometries sampled from the Born-Oppenheimer MD simulations. Computational details for the procedure are provided in Ref. 50.

Fig. 3c shows the ab initio simulation results for transient MSD, up to 1 ps, with various $\mathcal{Q}$ factors in the CPA framework and for a collective light-matter coupling strength that gives $\Omega_R = 260$ meV under the resonance condition. The raw data are presented with open circles, and the thin curves provide visual guidance. We see that the time-dependent MSDs resemble those measured in the experiments (see Fig. 2c in Ref. 2), validating our on-the-fly simulations of polariton transport dynamics with atomistic and ab initio details of the system. Experimentally, the MSD reported in Ref. 2 is based on the transient absorption measurements. The experimentally measured MSD reported in Ref. 2 was extracted from the transient differential transmission, and it was better connected through the following expression[7,9]

$$\sigma^2(t) = \sum_{n=1}^{N} \left(e^{\eta d |\psi(x_n,t)|^2} - 1 \right) \cdot (x_n - \langle \hat{x} \rangle)^2, \quad (12)$$

where η is the sample's absorption coefficient and d is the optical path length. These two parameters account for the difference between the actual MSD (defined in Eq. 10 and the experimentally extracted MSD from differential transmission measurements. The quantity $\exp\left(\eta d |\psi(x_n,t)|^2\right) - 1$ correlates to the transient differential transmission signal $\Delta T/T$ reported in experiments.[2,7] When $\eta d |\psi(x_n,t)|^2$ is small, which is satisfied by the polariton wave packets, the transient differential transmission signal is approximately $\exp\left(\eta d |\psi(x_n,t)|^2\right) - 1 \approx \eta d |\psi(x_n,t)|^2$, and the transient MSD becomes $\sigma^2(t) = \eta d \sum_{n=1}^{N} |\psi(x_n,t)|^2 \cdot (x_n - \langle \hat{x} \rangle)^2$; this expression is identical to the simulated MSD (Eq. 10) with a scaling factor of ηd. We found that $\eta d = 0.0222$ reproduces the transient MSD data in Ref. 2.

Fig. 4 shows the transient MSD of the polariton wavepacket, up to 1 ps, with various $\mathcal{Q}$ factors. We show $\lambda = 0.0017$ a.u., $\lambda = 0.0070$ a.u., and $\lambda = 0.014$ a.u. in Figs. 4a, 4b, and 4c respectively, corresponding to $\Omega_R = 50$ meV, $\Omega_R = 200$ meV, and $\Omega_R = 400$ meV. The black circles in Figs. 4b and 4c are the experimental data for Ref. 2 for $n = 6.5$ layers in the FP cavity. As the cavity loss rate Γ_c increases, the duration of the ballistic phase, characterized by a sharp increase in the MSD, decreases,

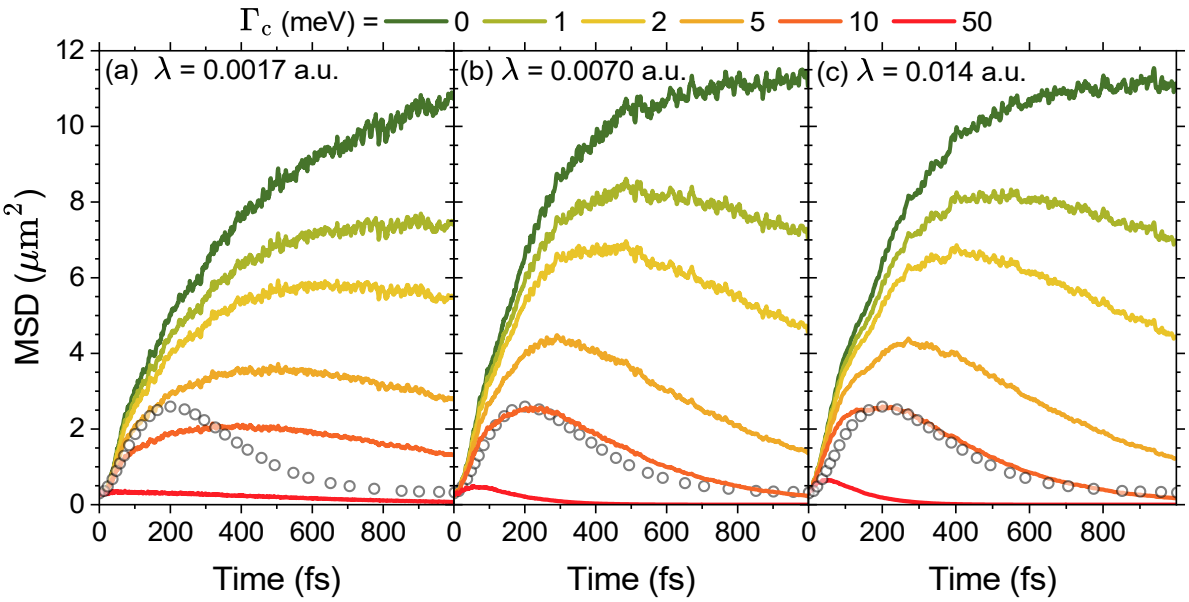

Figure 4: Mean-squared displacement (MSD) of the polariton wavepacket over time for various cavity quality factors Γ_c at collective light-matter coupling strength (a) $\Omega_R = 50$ meV ($\lambda = 0.0017$ a.u.), (b) $\Omega_R = 200$ meV ($\lambda = 0.0070$ a.u.), and (c) $\Omega_R = 400$ meV ($\lambda = 0.014$ a.u.). Black circles are experimental data (scaled) for $n = 6.5$ layers in Ref. 2.

in line with previous simulations and experimental measurements. The corresponding peak MSD also drops as Γ_c increases. Further, we see that experimental results are in close agreement with the ab initio simulations for a collective light-matter coupling strength Ω_R between 200 meV and 400 meV, and a cavity loss rate of $\Gamma_c = 10$ meV (see Figs. 4b and c).

For more general cases in polariton photochemistry or photophysics, the condition $|c_n(t)|^2 \ll 1$ may not always be fulfilled, especially for polariton photochemistry. In polariton photochemistry,[51] it was found that the polariton state quickly localizes onto one (or a few molecules), where $|c_n|^2$ is large, and a local bond-breaking process will happen on that molecule, which does sensitively depend on the excited state force. For polariton transport, from our results, we found that throughout all t, $|c_n|^2 \ll 1$ for transport dynamics. That said, for transport dynamics that could exhibit localization (due to various types of disorders, we can instead keep tracking each $|c_n(t)|^2$ in time and only start the excited state gradient calculation when $|c_m(t)|^2$ is larger than a certain threshold (*e.g.*, when the force contribution is in a range of $1 - 5\%$ of the ground state force), and still keep the CPA for all other $n \neq m$. This will still drastically save a lot of computational costs due to avoiding expensive excited-state gradients and derivative couplings.

In this letter, we demonstrate the validity of the classical path approximation in polariton quantum dynamics simulations. The fundamental reason why CPA works so well for polariton transport is that the polariton wave packet remains delocalized across a large number of molecules during the dynamics, making individual expansion coefficients $|c_n(t) \ll 1$. Thus, the excited state contribution to the nuclear force terms, which is proportional to $|c_n|^2$, will be negligibly small compared to the ground state forces. Neglecting the excited state contributions in on-the-fly simulations for polariton systems in the collective coupling regime is therefore a reasonable approximation. We have tested this approximation with HTC model systems, and the results of CPA are shown to be in excellent agreement with the dynamics with full nuclear gradients. We further use CPA to perform ab initio polariton transport simulations with BODIPY molecules coupled to cavity, with transient MSD results agree well with experiments.[2] This work paves the way towards using fully ab initio simulations to investigate polariton transport properties in experimentally relevant systems.

Acknowledgement This work was supported by the Department of Energy under Grant No. DE-SC0026212, the University of Rochester Pump-

Primer II funding, as well as by the University of Rochester Office of the Vice President for Research, the School of Medicine and Dentistry, and Arts, Sciences & Engineering via the Center for Integrated Research Computing (CIRC). B.X.K.C. appreciates support from the Elon Huntington Hooker Fellowship at the University of Rochester. B.M.W. appreciates the support of the Director's Postdoctoral Fellowship at Los Alamos National Laboratory (LANL), which is funded by the Laboratory Directed Research and Development (LDRD) at LANL. Computing resources were provided by the Center for Integrated Research Computing (CIRC) at the University of Rochester and the LANL Institutional Computing (IC) Program. P. H. appreciates valuable discussions with Andrew Musser.

References

(1) Balasubrahmaniyam, M.; Simkhovich, A.; Golombek, A.; Sandik, G.; Ankonina, G.; Schwartz, T. From enhanced diffusion to ultrafast ballistic motion of hybrid light–matter excitations. *Nature Materials* **2023**, *22*, 338–344.

(2) Pandya, R.; Ashoka, A.; Georgiou, K.; Sung, J.; Jayaprakash, R.; Renken, S.; Gai, L.; Shen, Z.; Rao, A.; Musser, A. J. Tuning the coherent propagation of organic exciton-polaritons through dark state delocalization. *Advanced Science* **2022**, *9*, 2105569.

(3) Xu, D.; Mandal, A.; Baxter, J. M.; Cheng, S.-W.; Lee, I.; Su, H.; Liu, S.; Reichman, D. R.; Delor, M. Ultrafast imaging of polariton propagation and interactions. *Nature Communications* **2023**, *14*, 3881.

(4) Jin, L.; Sample, A. D.; Sun, D.; Gao, Y.; Deng, S.; Li, R.; Dou, L.; Odom, T. W.; Huang, L. Enhanced two-dimensional exciton propagation via strong light–matter coupling with surface lattice plasmons. *ACS Photonics* **2023**, *10*, 1983–1991.

(5) Berghuis, A. M.; Tichauer, R. H.; de Jong, L. M.; Sokolovskii, I.; Bai, P.; Ramezani, M.; Murai, S.; Groenhof, G.; Gómez Rivas, J. Controlling exciton propagation in organic crystals through strong coupling to plasmonic nanoparticle arrays. *ACS photonics* **2022**, *9*, 2263–2272.

(6) Hong, Y.; Xu, D.; Delor, M. Exciton Delocalization Suppresses Polariton Scattering. *0*.

(7) Tichauer, R. H.; Sokolovskii, I.; Groenhof, G. Tuning the Coherent Propagation of Organic Exciton-Polaritons through the Cavity Q-factor. *Advanced Science* **2023**, *10*, 2302650.

(8) Chng, B. X.; Ying, W.; Lai, Y.; Vamivakas, A. N.; Cundiff, S. T.; Krauss, T. D.; Huo, P. Mechanism of Molecular Polariton Decoherence in the Collective Light–Matter Couplings Regime. *The Journal of Physical Chemistry Letters* **2024**, *15*, 11773–11783.

(9) Chng, B. X.; Mondal, M. E.; Ying, W.; Huo, P. Quantum Dynamics Simulations of Exciton Polariton Transport. *Nano Letters* **2025**,

(10) Zhou, Z.; Chen, H.-T.; Sukharev, M.; Subotnik, J. E.; Nitzan, A. Nature of polariton transport in a Fabry-Perot cavity. *Phys. Rev. A* **2024**, *109*, 033717.

(11) Sokolovskii, I.; Tichauer, R. H.; Morozov, D.; Feist, J.; Groenhof, G. Multi-scale molecular dynamics simulations of enhanced energy transfer in organic molecules under strong coupling. *Nature Communications* **2023**, *14*, 6613.

(12) Tutunnikov, I.; Qutubuddin, M.; Sadeghpour, H. R.; Cao, J. Characterization of Polariton Dynamics in a Multimode Cavity: Noise-enhanced Ballistic Expansion. `http://arxiv.org/abs/2410.11051`.

(13) Engelhardt, G.; Cao, J. Polariton Localization and Dispersion Properties of Disordered Quantum Emitters in Multimode Microcavities. *Phys. Rev. Lett.* **2023**, *130*, 213602.

(14) Suyabatmaz, E.; Ribeiro, R. F. Vibrational polariton transport in disordered media. *J. Chem. Phys.* **2023**, *159*, 034701.

(15) Aroeira, G. J. R.; Kairys, K. T.; Ribeiro, R. F. Coherent transient exciton transport in disordered polaritonic wires. *Nanophotonics* **2024**, *13*, 2553–2564.

(16) Krupp, N.; Groenhof, G.; Vendrell, O. Quantum Dynamics Simulation of Exciton-Polariton Transport. *16*, 5431.

(17) Ying, W.; Chng, B. X.; Delor, M.; Huo, P. Microscopic theory of polariton group velocity renormalization. *Nature Communications* **2025**, *16*, 6950.

(18) Sokolovskii, I.; Luo, Y.; Groenhof, G. Disentangling Enhanced Diffusion and Ballistic Motion of Excitons Coupled to Bloch Surface Waves with Molecular Dynamics Simulations. *16*, 6719–6727.

(19) Blackham, L.; Manjalingal, A.; Rahmanian Koshkaki, S.; Mandal, A. Microscopic Theory of Polaron-Polariton Dispersion and Propagation. *Nano Letters* **2025**, *25*, 15874–15882.

(20) Manjalingal, A.; Rahmanian Koshkaki, S.; Blackham, L.; Mandal, A. Tilted Material in an Optical Cavity: Light–Matter Moiré Effect and Coherent Frequency Conversion. *ACS Photonics* **2025**, *12*, —.

(21) Ghosh, P.; Manjalingal, A.; Wickramasinghe, S.; Rahmanian Koshkaki, S.; Mandal, A. Mean-field mixed quantum-classical approach for many-body quantum dynamics of exciton polaritons. *Physical Review B* **2025**, *112*, 104319.

(22) Liu, G.; Chen, H.-T. Dissecting Exciton-Polariton Transport in Organic Molecular Crystals: Emerging Conductivity Assisted by Intermolecular Vibrational Coupling. `http://arxiv.org/abs/2505.21888`.

(23) Fowler-Wright, P.; Reitz, M.; Yuen-Zhou, J. Mapping molecular polariton transport via pump-probe microscopy. *arXiv preprint* **2025**, preprint.

(24) Rahmanian Koshkaki, S.; Manjalingal, A.; Blackham, L.; Mandal, A. Exciton-Polariton Dynamics in Multilayered Materials. *arXiv preprint* **2025**, arXiv:2502.12933v2.

(25) Poddar, S.; Huo, P. Quantum Dynamics Simulations of Polariton Transport in a Bloch Surface Wave Cavity. *ChemRxiv* **2025**, Preprint.

(26) Zhou, W.; Hu, D.; Mandal, A.; Huo, P. Nuclear gradient expressions for molecular cavity quantum electrodynamics simulations using mixed quantum-classical methods. *The Journal of Chemical Physics* **2022**, *157*.

(27) Akimov, A. V.; Prezhdo, O. V. The PYXAID program for non-adiabatic molecular dynamics in condensed matter systems. *Journal of chemical theory and computation* **2013**, *9*, 4959–4972.

(28) Wang, L.; Akimov, A.; Prezhdo, O. V. Recent progress in surface hopping: 2011–2015. *The journal of physical chemistry letters* **2016**, *7*, 2100–2112.

(29) Kang, J.; Wang, L.-W. Nonadiabatic molecular dynamics with decoherence and detailed balance under a density matrix ensemble formalism. *Physical Review B* **2019**, *99*, 224303.

(30) Yamijala, S. S. R. K. C.; Huo, P. Direct Nonadiabatic Simulations of the Photoinduced Charge Transfer Dynamics. *J. Phys. Chem. A* **2021**, *125*, 628–635.

(31) Mandal, A.; Taylor, M. A.; Weight, B. M.; Koessler, E. R.; Li, X.; Huo, P. Theoretical advances in polariton chemistry and molecular cavity quantum electrodynamics. *Chemical Reviews* **2023**, *123*, 9786–9879.

(32) Tichauer, R. H.; Feist, J.; Groenhof, G. Multi-scale dynamics simulations of molecular polaritons: The effect of multiple cavity modes on polariton relaxation. *The Journal of Chemical Physics* **2021**, *154*, 104112.

(33) Taylor, M.; Mandal, A.; Huo, P. Light-Matter Interaction Hamiltonians in Cavity Quantum Electrodynamics. *ChemRxiv* **2024**, 10.26434/chemrxiv–2024–dklxd (accessed January 9, 2025).

(34) Koessler, E. R.; Mandal, A.; Huo, P. Incorporating Lindblad decay dynamics into mixed quantum-classical simulations. *The Journal of Chemical Physics* **2022**, *157*, 064101.

(35) Mondal, M. E.; Koessler, E. R.; Provazza, J.; Vamivakas, A. N.; Cundiff, S. T.; Krauss, T. D.; Huo, P. Quantum dynamics simulations of the 2D spectroscopy for exciton polaritons. *The Journal of Chemical Physics* **2023**, *159*, 094102.

(36) Hu, D.; Chng, B. X. K.; Ying, W.; Huo, P. Trajectory-based non-adiabatic simulations of the polariton relaxation dynamics. *J. Chem. Phys.* **2025**, *162*, 124113.

(37) Lee, M. K.; Huo, P.; Coker, D. F. Semiclassical path integral dynamics: Photosynthetic energy transfer with realistic environment interactions. *Annu. Rev. Phys. Chem.* **2016**, *67*, 639–668.

(38) Bossion, D.; Ying, W.; Chowdhury, S.; Huo, P. Non-adiabatic mapping dynamics in the phase space of the SU(N) Lie group. *J. Chem. Phys.* **2022**, *157*, 084105.

(39) Weight, B. M.; Mandal, A.; Huo, P. Ab initio symmetric quasi-classical approach to investigate molecular Tully models. *J. Chem. Phys.* **2021**, *155*, 084106.

(40) Mondal, M. E.; Vamivakas, A. N.; Cundiff, S. T.; Krauss, T. D.; Huo, P. Polariton spectra under the collective coupling regime. I. Efficient simulation of linear spectra and quantum dynamics. *J. Chem. Phys.* **2025**, *162*, 014114.

(41) Mondal, M. E.; Vamivakas, A. N.; Cundiff, S. T.; Krauss, T. D.; Huo, P. Polariton spectra under the collective coupling regime. II. 2D non-linear spectra. *J. Chem. Phys.* **2025**, *162*, 074110.

(42) Huo, P.; Coker, D. F. Communication: Partial linearized density matrix dynamics for dissipative, non-adiabatic quantum evolution. *The Journal of Chemical Physics* **2011**, *135*, 201101.

(43) Levine, B. G.; Martínez, T. J. Isomerization Through Conical Intersections. *Annu. Rev. Phys. Chem.* **2007**, *58*, 613–634.

(44) Curchod, B. F. E.; Martínez, T. J. Ab Initio Nonadiabatic Quantum Molecular Dynamics. *Chemical Reviews* **2018**, *118*, 3305–3336.

(45) Rana, B.; Hohenstein, E. G.; Martínez, T. J. Simulating the Excited-State Dynamics of Polaritons with Ab Initio Multiple Spawning. *The Journal of Physical Chemistry A* **2024**, *128*, 139–151.

(46) Hu, D.; Huo, P. Ab Initio Molecular Cavity Quantum Electrodynamics Simulations Using Machine Learning Models. *J. Chem. Theory Comput.* **2023**, *8*, 2353–2368.

(47) Frisch, M. J.; Trucks, G. W.; Schlegel, H. B.; Scuseria, G. E.; Robb, M. A.; Cheeseman, J. R.; Scalmani, G.; Barone, V.; Petersson, G. A.; Nakatsuji, H. et al. Gaussian˜16 Revision C.01. 2016; Gaussian Inc. Wallingford CT.

(48) Dewar, M. J. S.; Zoebisch, E. G.; Healy, E. F.; Stewart, J. J. P. Development and use of quantum mechanical molecular models. 76. AM1: a new general purpose quantum mechanical molecular model. *Journal of the American Chemical Society* **1985**, *107*, 3902–3909.

(49) Weight, B. M.; Mandal, A.; Huo, P. Semiclassical Quantum Dynamics (SQD). 2023; `https://github.com/bradenmweight/SQD`, original-date: 2023-01-15T22:28:05Z.

(50) Weight, B.; Rury, A.; Shao, Y.; Huo, P. Ab Initio Polariton Spectra of ZnTPP Molecules Collectively Coupled inside an Optical Cavity. 2025; `https://chemrxiv.org/engage/chemrxiv/article-details/6939caa0ef27c95d3bf282d8`.

(51) Dutta, A.; Tiainen, V.; Sokolovskii, I.; Duarte, L.; Markešević, N.; Morozov, D.; Qureshi, H. A.; Pikker, S.; Groenhof, G.; Toppari, J. J. Thermal disorder prevents the suppression of ultra-fast photochemistry in the strong light-matter coupling regime. *Nature Communications* **2024**, *15*, 6600.